ACS APPLIED MATERIALS & INTERFACES

Research Article

www.acsami.org

High-Performance $ZnCo_2O_4$@CeO_2 Core@shell Microspheres for Catalytic CO Oxidation

Fan Wang,[†,‡] Xiao Wang,[†] Dapeng Liu,*[,†] Jiangman Zhen,[†,‡] Junqi Li,[†,‡] Yinghui Wang,[†] and Hongjie Zhang*[,†]

[†]State Key Laboratory of Rare Earth Resource Utilization, Changchun Institute of Applied Chemistry, Chinese Academy of Sciences, Changchun, 130022 Jilin, China

[‡]Graduate University of Chinese Academy of Sciences, Beijing 100039, P.R. China

Supporting Information

ABSTRACT: In this paper, we report a self-assembly method to synthesize high-quality $ZnCo_2O_4$@CeO_2 core@shell microspheres with tunable CeO_2 thickness. $ZnCo_2O_4$ spheres were first synthesized as the core, followed by a controlled CeO_2 shell coating process. The thickness of CeO_2 shell could be easily tuned by varying the feeding molar ratio of Ce/Co. Transmission electron microscope (TEM) images and scanning transmission electron microscope (STEM) image have identified the core@shell structure of these samples. In CO oxidation tests these $ZnCo_2O_4$@CeO_2 core@shell microspheres exhibited promising catalytic performance, and the catalytic activity of the best sample is even close to the traditional noble metal-CeO_2 system, attaining 100% CO conversion at a relatively low temperature of 200 °C. Cycling tests confirm their good stability of these core@shell microspheres besides activity. Their high catalytic performance should be attributed to the core@shell structure formation, and moreover further H_2—temperature-programmed reduction (TPR) results revealed the possible synergistic effects between the two components of $ZnCo_2O_4$ and CeO_2.

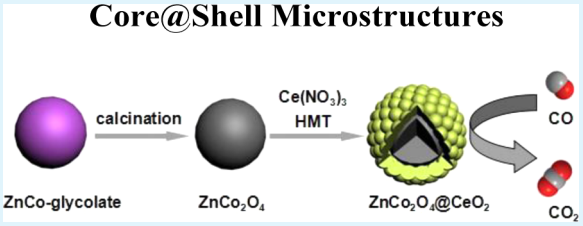

KEYWORDS: *$ZnCo_2O_4$, CeO_2, core@shell, microspheres, CO oxidation*

1. INTRODUCTION

In recent years, research interest has been aroused worldwide toward the development of self-assembly synthesis of CeO_2-based noble metal nanocatalysts for catalytic CO oxidation.[1−5] However, the quite high price level of noble metals and rare-earth oxides limits their further applications.[6−9] Therefore, it seems quite an issue to explore "noble metal-free" catalysts with well controlled particle size, shape, and structure as well as promising catalytic properties. Recent research shows that the hybrids composed by transition metal oxides (MOs) and CeO_2 exhibit high catalytic activity in CO oxidation, including CeO_2−CuO,[10,11] CeO_2−MnO_2,[12] CeO_2−NiO,[13] CeO_2−Fe_2O_3,[14] CeO_2−ZnO,[15] and CeO_2−Co_3O_4[16] systems, and among them CeO_2−CuO and CeO_2−Co_3O_4 are of better catalytic performance (Table S1). However, stability is a big problem for CuO that is apt to be etched seriously by H^+, OH^-, Cl^-, NH_4^+, etc. Our group has thus been focusing on the synthesis of the more stable CeO_2−Co_3O_4 system, and the obtained Co_3O_4@CeO_2 core@shell nanocubes exhibited rather good performance on catalytic CO oxidation.[16] However, this Ce−Co system remains two disadvantages: (1) Severe aggregation of Co_3O_4@CeO_2 core@shell nanocubes has been observed, which can be attributed to the bad monodispersity of Co_3O_4 seeds.[17−19] (2) Although Ce is almost the cheapest one among all the rare-earth elements, it is still much more expensive than most transition metals. The high Ce content of the CeO_2−Co_3O_4 hybrids will certainly increase the overall cost.

A reasonable solution is considered by using cobaltite (MCo_2O_4) which is thought to be a structure of partially substituted Co_3O_4 by another kind of transition metal to replace Co_3O_4 to form hybrids with CeO_2. These MCo_2O_4 structures not only have good monodispersity,[20−23] but the coupling of two metal species could also render MCo_2O_4 with rich redox reactions and hence improve their chemical or physical properties.[24−29] Zhu et al.[30] synthesized MCo_2O_4 (M = Cu, Mn, Ni) spinels with high surface area using mesoporous SBA-15 as the hard template. However, this synthetic route involves a multistep process, which is time-consuming and relatively complicated since it is well accepted that the CO oxidation process takes place at the interface of CeO_2 and metal oxide components.[31] Another solution for optimizing the fraction of interface of the two components is to prepare core@shell structures.[32] This core@shell structure can provide a great opportunity for controlling the interaction among the different components in ways that might boost structural stability or catalytic activity. Our previous work has identified that Co_3O_4@CeO_2 core@shell structures showed good catalytic

Received: August 31, 2014
Accepted: November 21, 2014
Published: November 21, 2014

activity for the oxidation of CO, and the synergistic effect between Co_3O_4 and CeO_2 should be responsible for the enhanced catalytic performance in CO oxidation.[16]

In this paper, we report a self-assembly method to synthesize high-quality $ZnCo_2O_4$@CeO_2 core@shell microspheres with tunable CeO_2 thickness. $ZnCo_2O_4$ spheres were first synthesized as the core,[24] followed by a controlled CeO_2 shell coating process. The thickness of this CeO_2 shell could be easily tuned by varying the feeding molar ratio of Ce/Co. Then the as-obtained $ZnCo_2O_4$@CeO_2 catalysts were studied in depth to find the optimal structure that showed the best catalytic performance on CO oxidation.

2. EXPERIMENTAL SECTION

Synthesis of $ZnCo_2O_4$ Microspheres. ZnCo-glycolate microspheres were synthesized by a simple refluxing process which has been reported before.[24] 1 mmol of $Zn(CH_3COO)_2{\cdot}2H_2O$ and 2 mmol of $Co(CH_3COO)_2{\cdot}4H_2O$ were dissolved in 50 mL of ethylene glycol (EG) under stirring at 50 °C for about 30 min and then refluxed at 170 °C for 2 h. The purple precipitate was collected and washed with acetone and ethanol for three times, followed by vacuum-drying at 60 °C overnight. To obtain $ZnCo_2O_4$ microspheres, the ZnCo-glycolate precursors were further calcined at 350 °C for 5 h with a ramp rate of 5 °C min^{-1} under atmospheric conditions.

Synthesis of $ZnCo_2O_4$@CeO_2 Core@shell Microspheres. 50 mg of $ZnCo_2O_4$ microspheres was ultrasonically dispersed in a mixed solution of 80 mL of water/ethanol (1:1 v/v), and then 0.05 mmol of $Ce(NO_3)_3$ and 0.1 mmol of hexamethylenetetramine (HMT) were added in turn. Afterward the temperature of the mixture was increased to 60 °C, and the mixture was refluxed for 2 h before being cooled to room temperature. The products were purified by centrifugation and washed with water and ethanol three times, followed by vacuum-drying at 60 °C. The as-obtained product was named as $ZnCo_2O_4$@CeO_2-0.05, while $ZnCo_2O_4$@CeO_2-0.1 and $ZnCo_2O_4$@CeO_2-0.2 were prepared in a similar method, except changing the $Ce(NO_3)_3$/HMT amount to 0.1 mmol of $Ce(NO_3)_3$/0.2 mmol HMT and 0.2 mmol of $Ce(NO_3)_3$/0.4 mmol HMT, respectively.

Synthesis of Pure CeO_2 Nanoparticles (NPs). One mmol $Ce(NO_3)_3$ was dissolved in a mixed solution of 20 mL of water and 20 mL of ethanol. After that, 25 mL of 0.02 g/mL HMT solution was added into the solution. The temperature of the mixture was increased to 70 °C, and the mixture was refluxed for 2 h before being cooled to room temperature. The products were purified by centrifugation and washed with water three times and then dried at 60 °C. Finally, the products were calcined in air at 400 °C for 3 h.

Characterization. The X-ray diffraction (XRD) patterns of the products were collected on a Rigaku-D/max 2500 V X-ray diffractometer with Cu.K_α radiation (λ = 1.5418 Å), with an operation voltage and current maintained at 40 kV and 40 mA. Transmission electron microscopic (TEM) images were obtained with a TECNAI G2 high-resolution transmission electron microscope operating at 200 kV. X-ray photoelectron spectroscopy (XPS) measurements were taken on an ESCALAB-MKII 250 photoelectron spectrometer (VG Co.) with Al.K_α X-ray radiation as the X-ray source for excitation. Inductively coupled plasma (ICP) analyses were performed with a Varian Liberty 200 spectrophotometer to determine the Ce, Zn, and Co contents. H_2-temperature-programmed reduction (TPR) was conducted on a TPDRO 1100 apparatus supplied by the Thermo-Finnigan Company. Before detection by the TCD, the gas was purified by a trap containing CaO + NaOH materials in order to remove H_2O and CO_2. For each time, 30 mg of the sample was heated from room temperature to 900 °C at a rate of 10 °C/min. A gaseous mixture of 5 vol % H_2 in N_2 was used as reductant at a flow rate of 20 mL/min. Micromeritics ASAP2020 surface area analyzer was used to measure gas adsorption. The solvent exchanged samples were activated and dried under vacuum at 150 °C for 15 h. Then before the measurement, the samples were dried again by using the "outgas" function of the surface area analyzer for 12 h at 150 °C to remove all residue solvents in the channels. A sample of about 120 mg was used for N_2 adsorption measurement and was maintained at 77 K with liquid nitrogen.

Catalytic Tests. Thirty mg of catalyst were put in a stainless steel reaction tube. The CO oxidation catalytic tests were performed under conditions in 1% CO and 20% O_2 in N_2 at a fixed space velocity of 30 mL/min. The composition of the gas was monitored online by gas chromatography.

3. RESULTS AND DISCUSSION

Scheme 1 depicts the strategy for synthesizing $ZnCo_2O_4$@CeO_2 microspheres. Uniform ZnCo-glycolate microspheres were first acquired by a refluxing method without addition of any surfactant or precipitant and served as the precursor to produce the $ZnCo_2O_4$ microspheres. Then the following step-by-step self-assembly process was used to deposit CeO_2 nanoparticles (NPs) on the surface of the preprepared $ZnCo_2O_4$ microspheres to form the final $ZnCo_2O_4$@CeO_2 core@shell microspheres.

Scheme 1. Schematic Illustration of the Formation of $ZnCo_2O_4$@CeO_2 Core@shell Microspheres

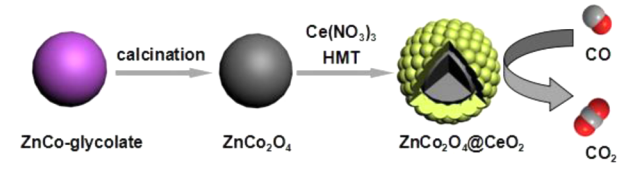

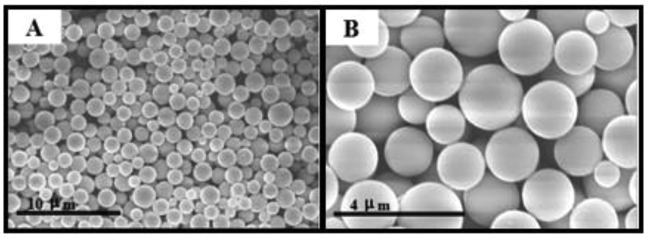

Figure 1. SEM images of ZnCo-glycolate microspheres.

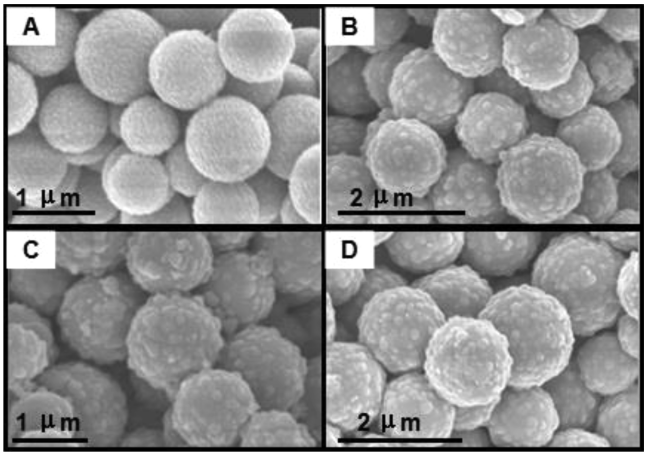

Figure 2. SEM images of (A): pure $ZnCo_2O_4$; (B): $ZnCo_2O_4$@CeO_2-0.05; (C): $ZnCo_2O_4$@CeO_2-0.1; (D): $ZnCo_2O_4$@CeO_2-0.2.

From the low magnification scanning electron microscopy (SEM) image in Figure 1, it can be seen that the ZnCo-glycolate precursor consists of uniform microspheres which is in accordance with the previous report.[24] The size distribution of the sample in Figure S1 indicates its average size of 1.63 μm.

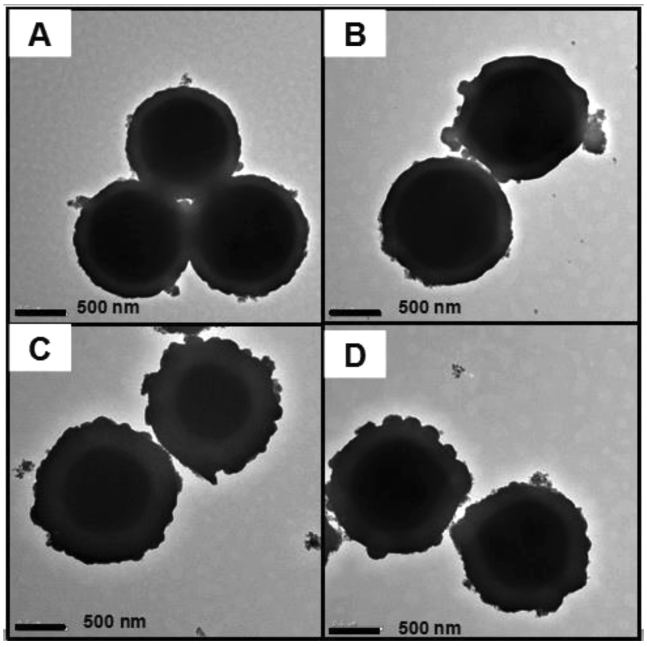

Figure 3. TEM images of $ZnCo_2O_4$@CeO_2 microspheres. (A): $ZnCo_2O_4$@CeO_2-0.05; (B): $ZnCo_2O_4$@CeO_2-0.1; (C): $ZnCo_2O_4$@CeO_2-0.2; (D): $ZnCo_2O_4$@CeO_2-0.1 (after ten cycles of CO oxidation).

Then we tried to coat CeO_2 NPs on the surface of ZnCo-glycolate microspheres directly by adding Ce, HMT, and ammonium hydroxide, but these ZnCo-glycolate microspheres are not stable in the presence of NH_4^+ that most of them were broken (Figure S2). It indicates that ZnCo-glycolate microspheres could not put up with the working condition with NH_4^+. Thus, the solid ZnCo-glycolate microspheres were then calcined to prepare more stable $ZnCo_2O_4$ at 350 °C for 5 h under atmospheric conditions (Figure 2A). The average size of the as-obtained pure $ZnCo_2O_4$ microspheres is about 1.5 μm (Figure S3).

The SEM images (Figure 2) show that after adding $Ce(NO_3)_3$ into the $ZnCo_2O_4$ solution and refluxing for 2 h, the surface of the $ZnCo_2O_4$ microspheres began to get rough indicating the successful surface deposition of CeO_2 components. By varying the feeding ratios, the thickness of surface deposited CeO_2 components can be tuned. In Figures S4, S5, and S6, it shows that $ZnCo_2O_4$@CeO_2-0.05, $ZnCo_2O_4$@CeO_2-0.1, and $ZnCo_2O_4$@CeO_2-0.2 have average sizes of 1.55 μm, 1.61 μm, and 1.68 μm, respectively. TEM images (Figure 3) also show that the final hybrids well maintained their initial microsphere structures. However, a high contrast between the outer shell and the inner core can be observed, firmly indicating their core@shell structure of the $ZnCo_2O_4$@CeO_2 hybrids. The high-resolution TEM image in Figure 4 shows that each $ZnCo_2O_4$ microsphere is coated by a dense layer built up by hundreds of ultrasmall CeO_2 NPs (<10 nm). In Figure 4B, the lattice spacing of 0.27 and 0.31 nm correspond well to the characteristic (200) and (111) planes of fluorite-phase CeO_2, respectively. However, these surface coated CeO_2 NPs were not stable under strong electron beams; it is hard for us to acquire their fast Fourier transform diffraction points as well as accurately measure the core and the shell. So the thickness of CeO_2 can be only roughly calculated from SEM images by measuring the difference between the $ZnCo_2O_4$@CeO_2 microspheres and the original naked $ZnCo_2O_4$ ones, and the results are shown in Table S3 in the Supporting Information.

Energy-dispersive X-ray spectroscopy (EDX) analyses in Figure 5 show that the body of the microspheres is composed of elements Zn, Co, Ce, and O. The core@shell microstructure could be further distinguished by mapping analysis (Figure 5, bottom right). It can be seen that elements Zn and Co only exist in the core position of the sphere, and element Ce is dilutedly dispersed but evenly located on the whole sphere that is a typical shell-structure feature. The result is just in good accordance with the TEM analyses. The STEM line-scan spectra (Figure 6) across the $ZnCo_2O_4$@CeO_2-0.1 microspheres was then carried out to further prove the core@shell geometry of the particles. This result reflects the higher atomic numbers of Zn and Co concentrate in the center of the sphere while Ce in the outer shell. The presence of the Zn−Co core and Ce shell is thus clearly confirmed.

The XRD patterns (Figure 7) provide the crystallinity and phase information on pure $ZnCo_2O_4$, pure CeO_2, and $ZnCo_2O_4$@CeO_2-0.05 to $ZnCo_2O_4$@CeO_2-0.2. The peaks at 2θ = 31.2°, 36.8°, 44.7°, 59.3°, and 65.1° correspond well to the characteristic (220), (311), (400), (511), and (440) reflections

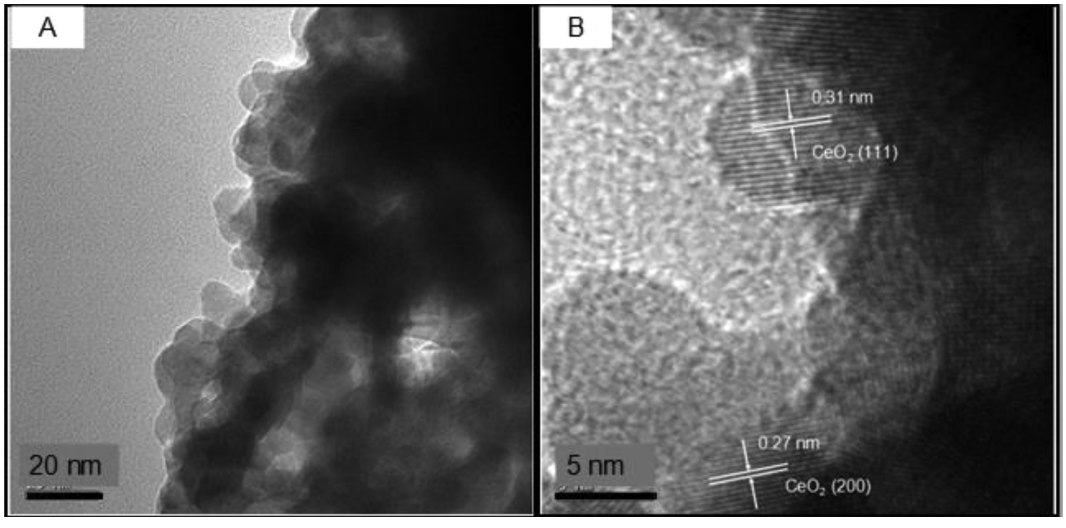

Figure 4. TEM images of the surface of the $ZnCo_2O_4$@CeO_2-0.1 microsphere.

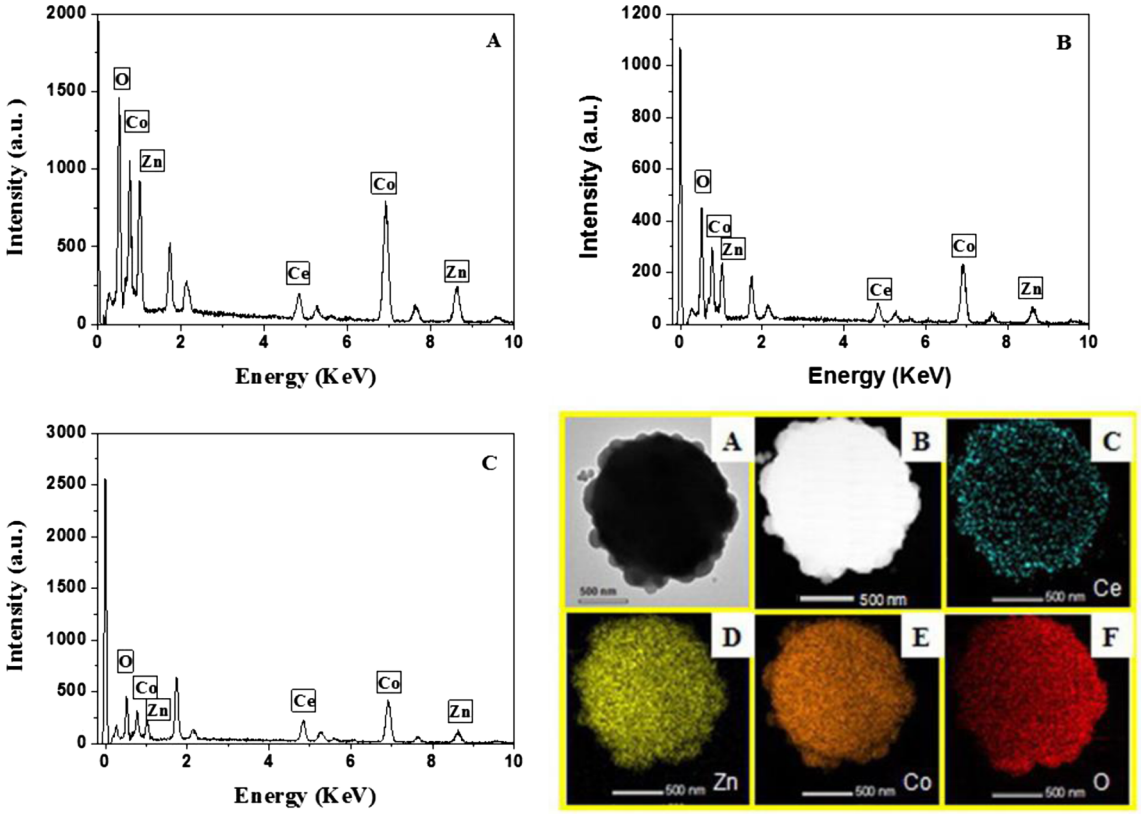

Figure 5. EDX spectra of $ZnCo_2O_4$@CeO_2-0.05 to $ZnCo_2O_4$@CeO_2-0.2 (A to C); TEM images and its mapping analysis of $ZnCo_2O_4$@CeO_2-0.1 (bottom right).

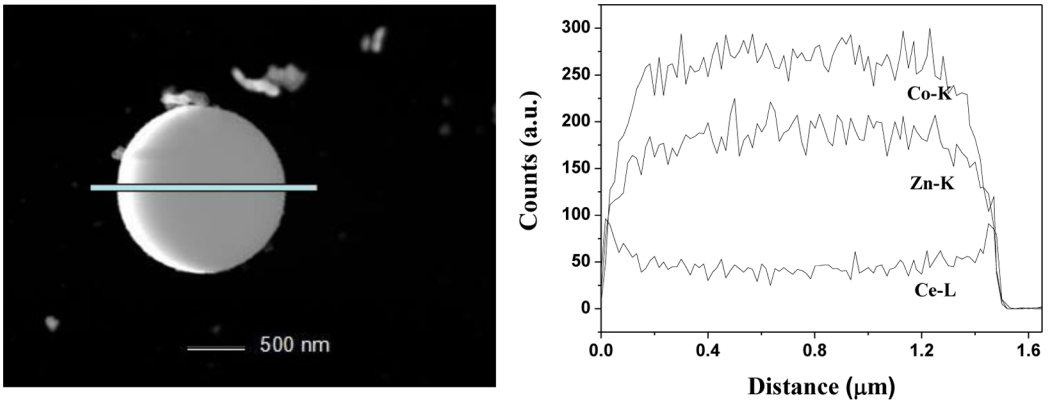

Figure 6. STEM-HAADF image of a core@shell microsphere and line profile obtained along the line.

of spinel-phase $ZnCo_2O_4$, respectively (JCPDS No. 23-1390). While the peaks at 2θ = 28.5°, 33.0°, 47.4°, and 56.4° can be indexed into the characteristic (111), (200), (220), and (311) reflections of fluorite-phase CeO_2, respectively (JCPDS No. 43-1002). However, the related peaks of CeO_2 seem broader compared with those of $ZnCo_2O_4$ indicating the shell is composed of smaller sized CeO_2 NPs.

XPS analysis (Figure 8) identifies the existence of Ce in the three hybrids of $ZnCo_2O_4$@CeO_2-0.05 to $ZnCo_2O_4$@CeO_2-0.2, because the two peaks of 882.8 and 899.5 eV correspond to the Ce $3d_{5/2}$ and Ce $3d_{3/2}$ spin−orbit peaks of CeO_2, respectively.[16] However, no Co and Zn signals can be found. As previously reported, the XPS curve of Co 2p shows two major peaks at 795.5 and 780.4 eV, corresponding to the Co $2p_{1/2}$ and Co $2p_{3/2}$ spin−orbit, respectively. Two major peaks lying at 1044.4 and 1021.3 eV are characteristic signals of Zn^{2+} with Zn $2p_{3/2}$ and Zn $2p_{1/2}$ orbits, respectively. It is known that the XPS characterization is only suitable for testing the superficial composition of samples, so the absence of Co and Zn signals can further demonstrate the core@shell structure of the as-obtained $ZnCo_2O_4$@CeO_2 microspheres, in good accordance with the results of the SEM and TEM analysis. ICP-MS analysis determines the Zn, Co, and Ce contents that the Ce contents are 3.71%, 7.40%, and 11.29% in molar ratio for $ZnCo_2O_4$@CeO_2-0.05 to $ZnCo_2O_4$@CeO_2-0.2, respectively, as shown in Table S2. It can be seen that the Ce content increases initially with the introduction of $Ce(NO_3)_3$ (Table S3). As previously reported,[16] the Ce content of the best Co_3O_4@CeO_2 sample is 25.23 mol %. Obviously $ZnCo_2O_4$@CeO_2-0.2 that has the largest Ce content in this

dx.doi.org/10.1021/am505853p | ACS Appl. Mater. Interfaces 2014, 6, 22216−22223

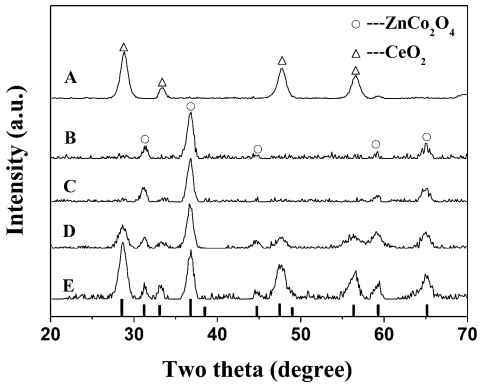

Figure 7. XRD patterns (A) pure CeO_2; (B) pure $ZnCo_2O_4$; (C) $ZnCo_2O_4$@CeO_2-0.05; (D) $ZnCo_2O_4$@CeO_2-0.1; (E) $ZnCo_2O_4$@CeO_2-0.2.

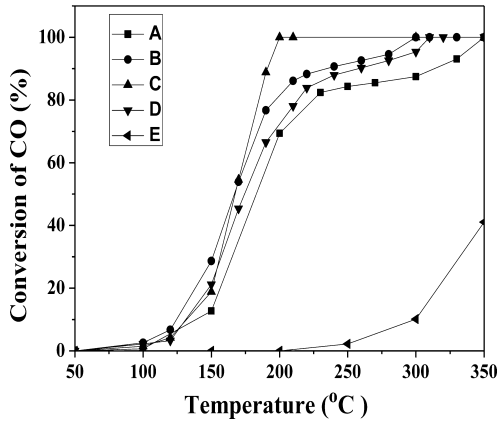

Figure 9. CO conversion curves (A): pure $ZnCo_2O_4$; (B): $ZnCo_2O_4$@CeO_2-0.05; (C): $ZnCo_2O_4$@CeO_2-0.1; (D): $ZnCo_2O_4$@CeO_2-0.2; (E): pure CeO_2.

work is still much lower than that of Co_3O_4@CeO_2. Besides, for $ZnCo_2O_4$@CeO_2-0.05 to $ZnCo_2O_4$@CeO_2-0.2, the molar ratio of Zn/Co is almost 1/2 which equals to the ideal stoichiometric ratio of the structure of $ZnCo_2O_4$.

To evaluate the catalytic activities of the three samples of $ZnCo_2O_4$@CeO_2-0.05, $ZnCo_2O_4$@CeO_2-0.1, and $ZnCo_2O_4$@CeO_2-0.2, catalytic CO oxidation was employed here as a model reaction. T_{100}, the temperature for 100% CO oxidation, is used to compare the catalytic activity of these samples. Figure 9 presents their CO conversion curves that it follows such a sequence of T_{100}: pure CeO_2 (limited activity) > pure $ZnCo_2O_4$ (350 °C) > $ZnCo_2O_4$@CeO_2-0.2 (310 °C) > $ZnCo_2O_4$@CeO_2-0.05 (300 °C) > $ZnCo_2O_4$@CeO_2-0.1 (200 °C). Obviously either pure $ZnCo_2O_4$ or CeO_2 shows much lower catalytic activity than these $ZnCo_2O_4$@CeO_2 microspheres. It has been reported that the catalytic activities of Co_3O_4 catalysts can be enhanced by forming hybrids with CeO_2 due to synergetic effects between Co_3O_4 and CeO_2.[16] Thus, it is reasonably concluded that the enhancement of $ZnCo_2O_4$@CeO_2 microspheres is probably caused by the similar synergistic effects between $ZnCo_2O_4$ and CeO_2. Besides, the far lower T_{100} (200 °C) of $ZnCo_2O_4$@CeO_2-0.1 indicates that in our case the optimal content of Ce might be around 7.40 mol % of Ce. Next, a cycling test was performed to study the stability of $ZnCo_2O_4$@CeO_2-0.1 (Figure 10). After ten successful cycles from 50 to 200 °C, $ZnCo_2O_4$@CeO_2-0.1 still maintained 100% conversion of CO into CO_2 at 200 °C (Cycling tests of $ZnCo_2O_4$@CeO_2-0.05 and $ZnCo_2O_4$@CeO_2-0.2 were listed in Figure S7.). SEM (Figure S8) and XRD (Figure S9) analyses

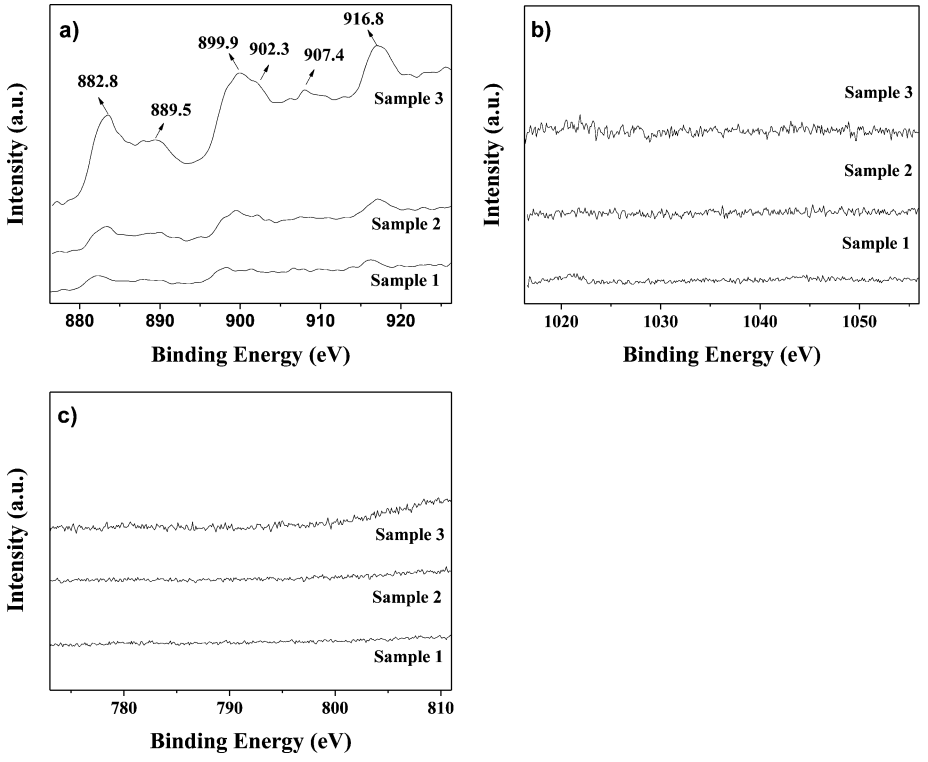

Figure 8. XPS analysis. a) Ce 3d core levels; b) Zn 2p core levels; c) Co 2p core levels of (Sample 1) $ZnCo_2O_4$@CeO_2-0.05, (Sample 2) $ZnCo_2O_4$@CeO_2-0.1, and (Sample 3) $ZnCo_2O_4$@CeO_2-0.2.

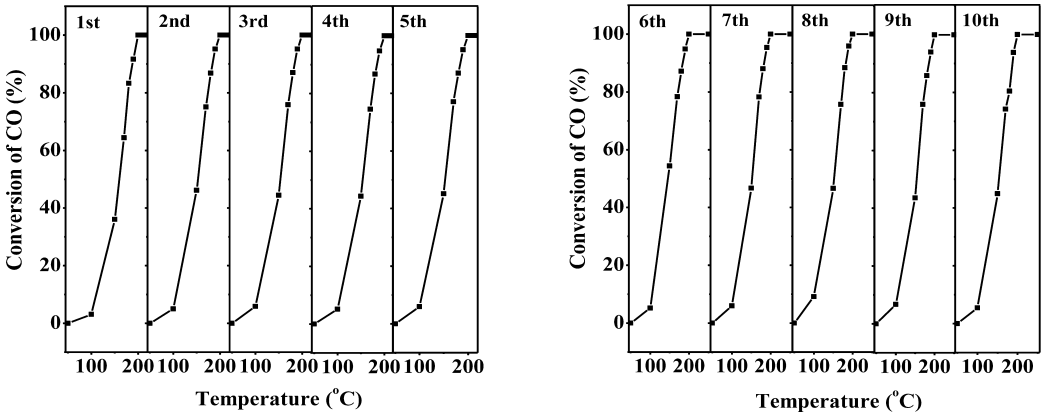

Figure 10. Cycling test of $ZnCo_2O_4$@CeO_2-0.1 for CO conversion.

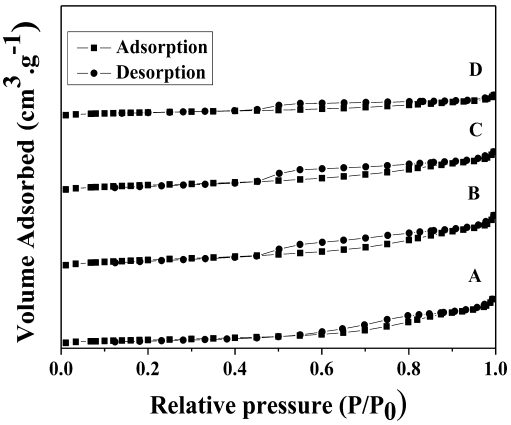

Figure 11. N_2 adsorption−desorption isotherm (A) $ZnCo_2O_4$; (B) $ZnCo_2O_4$@CeO_2-0.05; (C) $ZnCo_2O_4$@CeO_2-0.1; (D) $ZnCo_2O_4$@CeO_2-0.2.

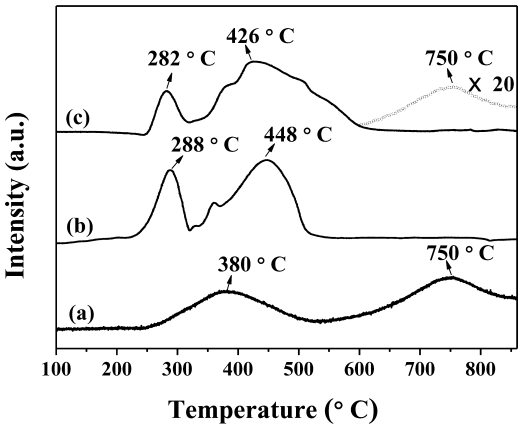

Figure 12. H_2-TPR profiles: (a): pure CeO_2; (b): pure $ZnCo_2O_4$; (c): $ZnCo_2O_4$@CeO_2-0.1.

demonstrate that the structure of $ZnCo_2O_4$@CeO_2-0.1 remained stable after catalytic cycles.

The N_2 adsorption−desorption isotherm curves are shown in Figure 11. It can be seen that all samples exhibit type-IV adsorption isotherms with a clear hysteresis loop in the relative pressure range of 0.4−1.0, indicating the presence of a mesoporous structure in the samples. Their BET surface areas are listed in Table 1; however, there is no evidence to suggest that the catalytic performance mainly depends on these data that the one with the largest surface areas show the best catalytic activity.

In order to study the synergetic effects of $ZnCo_2O_4$ and CeO_2,[31,32] the catalysts were investigated by H_2-TPR, and the results are displayed in Figure 12. For the fresh catalyst, the following reaction might be involved in the H_2-TPR process:

$$ZnCo_2O_4 + H_2 \rightarrow ZnO + 2CoO + H_2O \quad (1)$$

$$CoO + H_2 \rightarrow Co + H_2O \quad (2)$$

$$2CeO_2 + H_2 \rightarrow Ce_2O_3 + H_2O \quad (3)$$

Two broad TPR peaks observed at 380 and 750 °C for CeO_2 can be attributed to the reduction of surface capping oxygen and bulk oxygen of ceria, respectively.[27] The first two peaks at around 285 and 440 °C in Figure 12b and 12c could be attributed to the aforementioned two reduction steps of the $ZnCo_2O_4$ species.[28,29] When $ZnCo_2O_4$ microspheres were introduced, the reduction peaks shifted toward the lower temperature. By careful observation, it is found that the temperature of the first reduction peak and the second reduction peak for $ZnCo_2O_4$@CeO_2 are about 6 and 22 °C lower compared to pure $ZnCo_2O_4$, respectively, suggesting CeO_2 can improve the oxidizability of $ZnCo_2O_4$. The signal at 750 °C for CeO_2 seemed to disappear completely in the curve (c); however, if the temperature range of 600 to 900 °C was enlarged for 20 times, the peak at 750 °C for CeO_2 just appeared. It might be caused by the small amount of CeO_2 in $ZnCo_2O_4$@CeO_2.

4. CONCLUSION

In summary, we have demonstrated a self-assembly method for synthesis of $ZnCo_2O_4$@CeO_2 core@shell microspheres. The catalytic properties of the samples have been investigated

Table 1. BET Surface Areas of $ZnCo_2O_4$ and $ZnCo_2O_4$@CeO_2 Microspheres

sample	$ZnCo_2O_4$	$ZnCo_2O_4$@CeO_2-0.05	$ZnCo_2O_4$@CeO_2-0.1	$ZnCo_2O_4$@CeO_2-0.2
BET surface areas ($m^2 \cdot g^{-1}$)	37.4682	57.0575	49.9037	33.4925

systematically. The $ZnCo_2O_4$@CeO_2 core@shell microspheres show higher catalytic activities than either pure $ZnCo_2O_4$ or CeO_2, which can be attributed to synergistic effects between the two components. The CeO_2 shell thickness can be tuned by varying the usage amount of $Ce(NO_3)_3$, and $ZnCo_2O_4$@CeO_2-0.1 has an optimal Ce content (only one-third compared to our previously reported Co_3O_4@CeO_2) for the best catalytic activity, attaining 100% CO conversion at 200 °C. In addition, it shows a good catalytic stability during the CO oxidation process. It is believed that our $ZnCo_2O_4$@CeO_2 core@shell microspheres could be a promising candidate catalyst for CO oxidation. Thus, this work supplies an efficient way to optimize the catalytic performance by simply controlling the ratio between Ce and Co, which will surely benefit this kind of catalysts.

■ ASSOCIATED CONTENT

Supporting Information

Additional SEM images; XRD and ICP results. This material is available free of charge via the Internet at http://pubs.acs.org.

■ AUTHOR INFORMATION

Corresponding Authors

*Fax: 86-431-85698041. E-mail: liudp@ciac.ac.cn.
*E-mail: hongjie@ciac.ac.cn.

Notes

The authors declare no competing financial interest.

■ ACKNOWLEDGMENTS

This work was supported by the financial aid from the National Natural Science Foundation of China (Grant Nos. 91122030, 51272249, 21210001, 21401186, and 21221061) and the MOST of China (Grant No. 2014CB643802).

■ REFERENCES

(1) Bera, P.; Patil, K. C.; Jayaram, V.; Subbanna, G. N.; Hegde, M. S. Ionic Dispersion of Pt and Pd on CeO_2 by Combustion Method: Effect of Metal-Ceria Interaction on Catalytic Activities for NO Reduction and CO and Hydrocarbon Oxidation. *J. Catal.* **2000**, *196*, 293−301.

(2) Zhang, Y. H.; Zhang, N.; Tang, Z. R.; Xu, Y. J. A Unique Silk Mat-Like Structured Pd/CeO_2 As An Efficient Visible Light Photocatalyst for Green Organic Transformation in Water ACS. *Sustainable Chem. Eng.* **2013**, *1*, 1258−1266.

(3) Wang, X.; Liu, D. P.; Song, S. Y.; Zhang, H. J. Pt@CeO_2 Multicore@Shell Self-Assembled Nanospheres: Clean Synthesis, Structure Optimization, and Catalytic Applications. *J. Am. Chem. Soc.* **2013**, *135*, 15864−15872.

(4) Satsuma, A.; Yanagihara, M.; Ohyama, J.; Shimizu, K. Oxidation of CO over Ru/Ceria Prepared by Self-Dispersion of Ru Metal Powderinto Nano-Sized Particle. *Catal. Today* **2013**, *201*, 62−67.

(5) Wang, X.; Liu, D. P.; Song, S. Y.; Zhang, H. J. Synthesis of Highly Active Pt-CeO_2 Hybrids with Tunable Secondary Nanostructures for the Catalytic Hydrolysis of Ammonia Borane. *Chem. Commun.* **2012**, *48*, 10207−10209.

(6) Ke, J.; Xiao, J. W.; Zhu, W.; Liu, H. C.; Si, R.; Zhang, Y. W.; Yan, C. H. Dopant-Induced Modification of Active Site Structure and Surface Bonding Mode for High-Performance Nanocatalysts: CO Oxidation on Capping-free (110)-oriented CeO_2:Ln (Ln = La−Lu) Nanowires. *J. Am. Chem. Soc.* **2013**, *135*, 15191−15200.

(7) Wang, Q.; Jia, W. J.; Liu, B. C.; Dong, A.; Gong, X.; Li, C. Y.; Jing, P.; Li, Y. J.; Xu, G. R.; Zhang, J. Hierarchical Structure Based on Pd(Au) Nanoparticles Grafted onto Magnetite Cores and Double Layered Shells: Enhanced Activity for Catalytic Applications. *J. Mater. Chem. A* **2013**, *1*, 12732−12741.

(8) Chen, S. F.; Li, J. P.; Qian, K.; Xu, W. P.; Lu, Y.; Huang, W. X.; Yu, S. H. Large Scale Photochemical Synthesis of M@TiO_2 Nanocomposites (M = Ag, Pd, Au, Pt) and Their Optical Properties, CO Oxidation Performance, and Antibacterial Effect. *Nano Res.* **2010**, *3*, 244−255.

(9) Jin, M. S.; Liu, H. Y.; Zhang, H.; Xie, Z. X.; Liu, J. Y.; Xia, Y. N. Synthesis of Pd Nanocrystals Enclosed by {100} Facets and with Sizes <10 nm for Application in CO Oxidation. *Nano Res.* **2011**, *4*, 83−91.

(10) Hornes, A.; Hungría, A. B.; Bera, P.; Camara, A. L.; García, M. F.; Arias, A. M.; Barrio, L.; Estrella, M.; Zhou, G.; Fonseca, J. J.; Hanson, J. C.; Rodriguez, J. A. Inverse CeO_2/CuO Catalyst As an Alternative to Classical Direct Configurations for Preferential Oxidation of CO in Hydrogen-Rich Stream. *J. Am. Chem. Soc.* **2010**, *132*, 34−35.

(11) Zeng, S. H.; Wang, Y.; Liu, K. W.; Liu, F. R.; Su, H. Q. CeO_2 Nanoparticles Supported on CuO with Petal-Like and Sphere-Flower Morphologies for Preferential CO Oxidation. *Int. J. Hydrogen Energy* **2012**, *37*, 11640−11649.

(12) Chen, G. Z.; Rosei, F.; Ma, D. L. Interfacial Reaction-Directed Synthesis of Ce-Mn Binary Oxide Nanotubes and Their Applications in CO Oxidation and Water Treatment. *Adv. Funct. Mater.* **2012**, *22*, 3914−3920.

(13) Sun, J. F.; Ge, C. Y.; Yao, X. J.; Cao, Y.; Zhang, L.; Tang, C. J.; Dong, L. Preparation of NiO/CeO_2 Catalysis by Solid State Impregnation and Their Application in CO Oxidation. *Acta Phys.-Chim. Sin.* **2013**, *29*, 2451−2458.

(14) Bao, H. Z.; Chen, X.; Fang, J.; Jiang, Z. Q.; Huang, W. X. Structure-activity Relation of Fe_2O_3 - CeO_2 Composite Catalysts in CO Oxidation. *Catal. Lett.* **2008**, *125*, 160−167.

(15) Xie, Q. H.; Zhao, Y.; Guo, H. Z.; Lu, A. L.; Zhang, X. X.; Wang, L. S.; Chen, M. S.; Peng, D. L. Facile Preparation of Well-Dispersed CeO_2-ZnO Composite Hollow Microspheres with Enhanced Catalytic Activity for CO Oxidation. *ACS Appl. Mater. Interfaces* **2014**, *6*, 421−428.

(16) Zhen, J. M.; Wang, X.; Liu, D. P.; Song, S. Y.; Wang, Z.; Wang, Y. H.; Li, J. Q.; Wang, F.; Zhang, H. J. Co_3O_4@CeO_2 Core@Shell Cubes: Designed Synthesis and Optimization of Catalytic Properties. *Chem.—Eur. J.* **2014**, *20*, 1−6.

(17) Mu, J. S.; Zhang, L.; Zhao, M.; Wang, Y. Catalase Mimic Property of Co_3O_4 Nanomaterials with Different Morphology and Its Application as a Calcium Sensor. *ACS Appl. Mater. Interfaces* **2014**, *6*, 7090−7098.

(18) Esswein, A. J.; McMurdo, M. J.; Ross, P. N.; Bell, A. T.; Tilley, T. D. Size-Dependent Activity of Co_3O_4 Nanoparticle Anodes for Alkaline Water Electrolysis. *J. Phys. Chem. C* **2009**, *113*, 15068−15072.

(19) Shen, L. S.; Wang, C. X. Hierarchical Co_3O_4 Nanoparticles Embedded in a Carbon Matrix for Lithium-Ion Battery Anode Materials. *Electrochim. Acta* **2014**, *133*, 16−22.

(20) Wu, H. B.; Pang, H.; Lou, X. W. Facile Synthesis of Mesoporous $Ni_{0.3}Co_{2.7}O_4$ Hierarchical Structures For High-Performance Supercapacitors. *Energy Environ. Sci.* **2013**, *6*, 3619−3626.

(21) Huang, L.; Chen, D. C.; Yong, D.; Feng, S.; Wang, Z. L.; Liu, M. L. Nickel-Cobalt Hydroxide Nanosheets Coated on $NiCo_2O_4$ Nanowires Grown on Carbon Fiber Paper for High-Performance Pseudocapacitors. *Nano Lett.* **2013**, *13*, 3135−3139.

(22) Yan, S. C.; Ouyang, S. X.; Gao, J.; Yang, M.; Feng, J. Y.; Fan, X. X.; Wan, L. J.; Li, Z. S.; Ye, J. H.; Zhou, Y.; Zou, Z. G. A Room-Temperature Reactive-Template Route to Mesoporous $ZnGa_2O_4$ with Improved Photocatalytic Activity in Reduction of CO_2. *Angew. Chem., Int. Ed.* **2010**, *49*, 6400−6404.

(23) Yuan, C. Z.; Li, J. Y.; Hou, L. R.; Lin, J. D.; Pang, G.; Zhang, L. H.; Lian, L.; Zhang, X. G. Template-Engaged Synthesis of Uniform Mesoporous Hollow $NiCo_2O_4$ Sub-Microspheres Towards High-Performance Electrochemical Capacitors. *RSC Adv.* **2013**, *3*, 18573−18578.

(24) Hu, L. L.; Qu, B. H.; Li, C. C.; Chen, Y. J.; Mei, L.; Lei, D. N.; Chen, L. B.; Li, Q. H.; Wang, T. H. Facile Synthesis of Uniform Mesoporous $ZnCo_2O_4$ Microspheres As A High-Performance Anode Material for Li-ion Batteries. *J. Mater. Chem. A* **2013**, *1*, 5596−5602.

(25) Li, J. F.; Wang, J. Z.; Wexler, D.; Shi, D. Q.; Liang, J. W.; Liu, H. K.; Xiong, S. L.; Qian, Y. T. Simple Synthesis of Yolk-shelled $ZnCo_2O_4$ Microspheres towards Enhancing the Electrochemical Performance of Lithium-Ion Batteries in Conjunction with a Sodium Carboxymethyl Cellulose Binder. *J. Mater. Chem. A* **2013**, *1*, 15292−15299.
(26) Sharma, Y.; Sharma, N.; Subba Rao, G. V.; Chowdari, B. V. R. Nanophase $ZnCo_2O_4$ as a High Performance Anode Material for Li-Ion Batteries. *Adv. Funct. Mater.* **2007**, *17*, 2855−2861.
(27) Qiu, Y. C.; Yang, S. H.; Deng, H.; Jin, L. M.; Li, W. S. A Novel Nanostructured Spinel $ZnCo_2O_4$ Electrode Material: Morphology Conserved Transformation from A Hexagonal Shaped Nanodisk Precursor and Application in Lithium Ion Batteries. *J. Mater. Chem.* **2010**, *20*, 4439−4444.
(28) Huang, T. F.; Mohamed, S. G.; Shen, C. C.; Tsai, Y. Q.; Chang, W. S.; Liu, R. S. Mesoporous $ZnCo_2O_4$ Nanoflakes with Bifunctional Electrocatalytic Activities toward Efficiencies of Rechargeable Lithium−Oxygen Batteries in Aprotic Media. *Nanoscale* **2013**, *5*, 12115−12119.
(29) Li, J. F.; Xiong, S. L.; Li, X. W.; Qian, Y. T. A Facile Route to Synthesize Multiporous $MnCo_2O_4$ and $CoMn_2O_4$ Spinel Quasi-Hollow Spheres with Improved Lithium Storage Properties. *Nanoscale* **2013**, *5*, 2045−2054.
(30) Zhu, J. K.; Gao, Q. M. Mesoporous MCo_2O_4 (M = Cu, Mn and Ni) Spinels: Structural Replication, Characterization and Catalytic Application in CO Oxidation. *Microporous Mesoporous Mater.* **2009**, *124*, 144−152.
(31) Luo, J. Y.; Meng, M.; Zha, Y. Q.; Guo, L. H. Identification of the Active Sites for CO and C_3H_8 Total Oxidation over Nanostructured Cu-CeO_2 and Co_3O_4-CeO_2 Catalysts. *J. Phys. Chem. C* **2008**, *112*, 8694−8701.
(32) Mitsudome, T.; Mikami, Y.; Matoba, M.; Mizugaki, T.; Jitsukawa, K.; Kaneda, K. Design of a Silver-Cerium Dioxide Core-Shell Nanocomposite Catalyst for Chemoselective Reduction Reactions. *Angew. Chem., Int. Ed.* **2012**, *51*, 136−139.